

The Effect of Electrode Morphology on Solid Oxide Fuel Cell Performance

J.G. Pharoah^a, L. Handl^b and V. Schmidt^b

^a Queen's-RMC Fuel Cell Research Centre, Queen's University, Kingston, ON, K7L 4T5,
CANADA

^b Institute of Stochastics, Ulm University, D-89069 Ulm, GERMANY

Three different electrode morphologies are generated from three different starting powders, spheres representing non aggregated powders, agglomerates of spheres and high aspect ratio cylinders modelling splats formed in plasma sprays. Electrodes from each morphology are analysed using finite volumes to predict the effective transport coefficients, the triple phase boundary length and the performance of the electrode. The same structures are also analysed using morphological characterization which can be much more efficient. It was found that high aspect ratio base particles are favourable, and that constrictivity correlates best with the finite volume transport calculations.

Introduction

Solid oxide fuel cells are often made with two distinct solid materials which are combined to form an electrode which conducts both ions and electrons and which has porosity to transport gases to the reaction sites. While the powders used to make such electrodes may be comprised of close to spherical base particles, the method of manufacturing the electrode may result in considerable changes in the final structure.

The morphology of a material has a great influence on its physical properties (1,2). Understanding this influence allows for a fast evaluation of new materials because determining geometrical properties of a material's morphology is often faster and easier than to measure or simulate its physical behaviour. Using stochastic models as developed in (3), which can represent a wide range of geometries, it can even be possible to establish quantitative relationships between morphological characteristics and physical parameters (4).

In this paper, we generate packings of three different types of particles. Spheres are chosen to represent minimal variations from the base powders during manufacturing and sintering, while agglomerates (collections of overlapping spheres) are used to represent particles which agglomerate at some stage during manufacturing and cylinders are used to represent an idealised form of the particle splats which are formed when electrodes are made by plasma spraying. We use methods from image analysis and spatial statistics as presented, e.g., in (5,6), to describe the morphology of these packings. The main focus is on the effect of the base particle shape on the morphology, and hence, on the physical properties of the material.

Geometry Generation

Geometries of random porous media are generated using a modified collective rearrangement algorithm (7), wherein the base particles are depicted in Figure 1. The base particle consists of a single sphere for the spherical packings, four overlapping component spheres equally distributed on the circumference of a circle of the same diameter as the component spheres for the agglomerate packings, and six spheres arranged in contact around a central seventh identical sphere in the case of cylindrical packings. In all cases the largest characteristic dimension of the base particle is $1\ \mu\text{m}$ and the particle aspect ratios are 1, $3/2$ and 3 for spheres, agglomerates and cylinders respectively.

The collective rearrangement algorithm initially randomly places an equal number of base particles of each desired solid phase which is larger than the final number of particles. The particles are then moved and rotated in a physical manner to eliminate particle overlaps greater than a set tolerance which is permitted to account for particle sintering. Particles which are moved repeatedly and which do not fit in the vicinity are randomly re-placed, whereas particles which do fit are slowly lowered until they touch other particles or the ground in order to achieve a stable packing. Finally, the domain is cut to desired size yielding a packing which is close to, but not quite a jammed packing. All calculations during packing are based upon the component spheres only, and hence the packing is exact for the spheres and the agglomerates, but approximate for the cylinders which are derived from and slightly larger than the component spheres (7).

In this work, 20 random packings were produced for each base particle shape. The domain used for the packing was a cube of approximately $19\ \mu\text{m}$ per side out of which a central cube of $16\ \mu\text{m}$ was extracted (17 and $14\ \mu\text{m}$ for the cylinders) in order to minimize any effects of the boundary. The base particle size of the ionically conducting phase and the electronically conducting phase was equal and the target solid volume fraction for each phase was 50% of the entire solid phase.

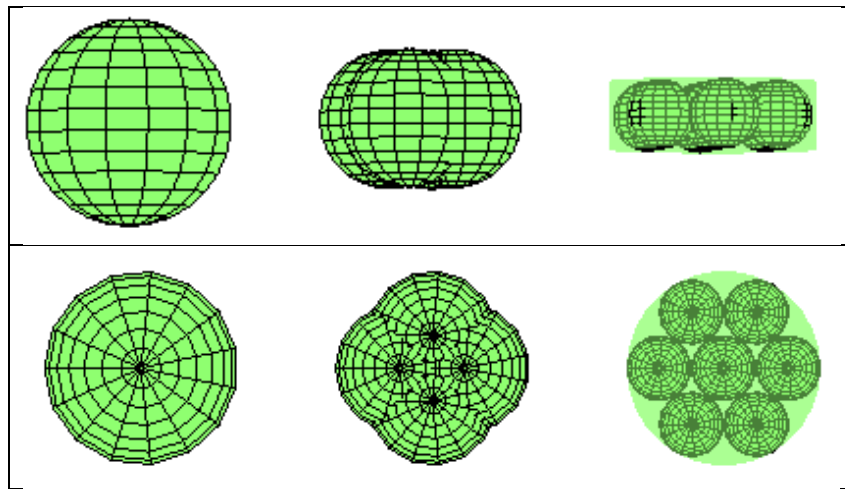


Figure 1. Side and top view of the base particles used to form the spheres, agglomerates and cylinders. In all cases the largest dimension is $1\ \mu\text{m}$.

Methods

Finite Volumes

A subset of the packing was meshed using a suitably modified version of the open source computational fluid dynamics package OpenFOAM. The mesh is body fitted and refined near solid surfaces to produce a discrete representation of the actual surfaces and interfaces present in the packings. Direct analysis of the mesh produces a measure of the porosity of the domains, the final volume fraction of each phase and the portion of each phase which is non-percolating with respect to the largest connected cluster of that phase.

OpenFOAM is then used to solve for the effective transport coefficient in each of the three percolating phases. This is carried out by solving a Laplace equation for conservation of mass, or charge (depending on the phase). This is repeated three times, for each phase to determine the effective transport coefficient in each coordinate direction and is carried out by prescribing a concentration or potential (depending on the phase) of zero on one face, a value of 1 on the opposite face and no-flux on the remaining four faces using a diffusivity or conductivity with a magnitude of 1. The solution then yields the transport rate of mass or charge through the domain, q . The effective transport coefficient is given by

$$\Gamma = q L \Gamma_o, \quad [1]$$

where L is the linear dimension of the domain and Γ_o is the known transport coefficient of the bulk phase. While Γ is used in reference to a general transport coefficient, diffusivity, D is considered in the pore phase, while the electronic and ionic conductivities, σ_e, σ_i respectively, are considered in the solid phases. In addition, the diffusivity is further limited in the gas phase by pore confinement effects which can be characterized by the Knudsen number, Kn , which is the ratio of a properly chosen characteristic length scale in the porous media, and the mean free path of gas at the operating pressure and temperature (8) such that

$$D_i = D^{\text{eff}} / (1 + Kn). \quad [2]$$

where D_i is the diffusivity accounting for the porous geometry and pore constriction effects while D^{eff} is the diffusivity solved in OpenFOAM accounting only for the pore geometry. The current production in an SOFC anode is also predicted by solving the coupled transport of hydrogen in the pore phase, electrons in the electronically conducting solid phase and oxide ions in the ionically conducting solid phase. Reactions occur at the triple phase boundaries according to

$$i = i_o \lambda_{tpb} \left[\exp\left(\frac{\alpha_a F \eta_{act}}{RT}\right) - \exp\left(-\frac{\alpha_c F \eta_{act}}{RT}\right) \right], \quad [3]$$

where i_o is the exchange current density, λ_{tpb} is the length of the triple phase boundary, α is the charge transfer coefficient, η_{act} is the local over-potential, F is Farady's constant, R is the gas constant and T is the local temperature. The exchange current density is a function of the local concentration and the activation over-potential, η_{act} , is a function of

the local potentials. Simulations are carried out for a mixture of 97% H₂ and 3% H₂O at atmospheric pressure and 800°C. Details of the performance model and data used for kinetics and material properties are given in (9) and (10).

Morphological Characteristics

The same subsets of the packings as in the previous section have been analysed geometrically in order to find purely morphological characteristics of the particle systems which clearly influence transport. For this purpose, the packings have been discretized on a voxel grid with a voxel side length of 0.02 μm (50 voxels per particle diameter). We considered the mean geometric tortuosity, the mean chord length, and the constrictivity of each phase.

The geometric tortuosity describes the windedness of paths through a phase and is defined as follows: Consider a voxel x of the phase of interest on one of the faces of the cubical domain. We are interested in the shortest path \overline{xy} from x to a voxel on the opposite face of the domain, say y , visiting only voxels of the same phase. The geometric tortuosity, measured from starting voxel x , is defined as the length of the path \overline{xy} divided by the side length of the cube. Averaging the geometric tortuosity over all possible starting voxels, which are the voxels of the phase of interest lying on the boundary of the domain, yields a mean value for the geometric tortuosity of this phase.

To measure the mean chord length of a phase we consider all lines parallel to the coordinate axes of the voxel grid which are represented by one straight line of voxels. Intersecting the line with the phase of interest yields line segments. The mean chord length of a phase is the average over the length of the segments obtained for all these lines.

The constrictivity, β , is a structural characteristic quantifying bottleneck effects within a phase. It takes values between 0 and 1 with values close to 1 indicating little and values close to 0 indicating strong bottleneck effects. We consider the parameter as used, e.g., in (4) and (3), which is defined as $\beta = r_{min}^2/r_{max}^2$. Here, r_{min} is the radius such that exactly 50 % of the phase volume can be covered with (overlapping) spheres with radius r_{min} , which are placed into the phase of interest coming from one side of the domain. The other radius, r_{max} , is the median radius obtained from the continuous phase size distribution. Thus, the constrictivity is a directed quantity, though in this work we considered an average over all coordinate directions. Intuitively, β can be interpreted as the quotient of the surface area of a typical cross section through a bottle neck divided by the surface area of a typical cross section through a bulge. For more details regarding these morphological characteristics, see eg., (3,4,11).

Results

Figure 2 shows one of the 20 independent samples generated for each of the three types of base particles: spheres, agglomerates and cylinders. In all cases the light green colour represents the ion conducting phase, the grey indicates the electron conducting phase. The dark green colour represents isolated clusters of ion conducting material while yellow indicates isolated clusters of electron conducting material. These clusters are a

barrier to gas transport, but do not participate in charge transport or contribute to the triple phase boundary length.

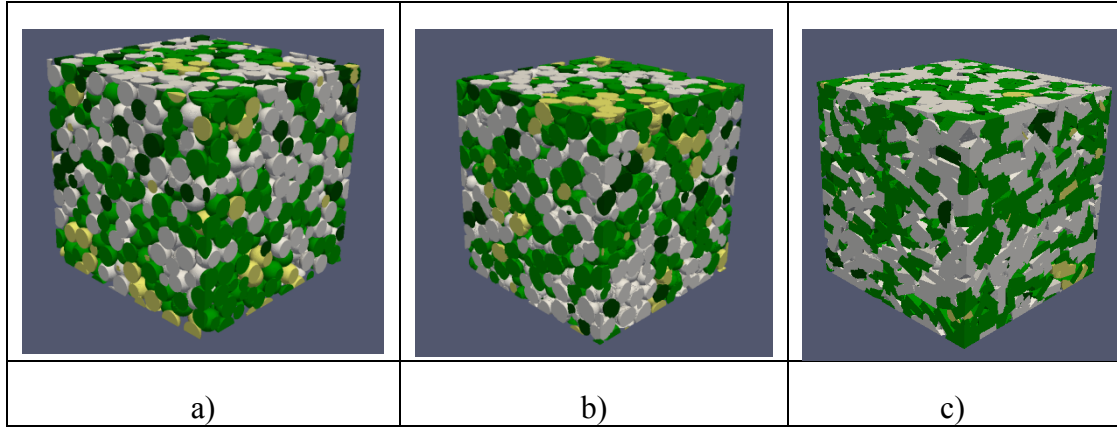


Figure 2. Solid phase geometry of a) spheres, b) agglomerates and c) cylinders. In all cases light green is the percolated ionic conductor, dark green is the un-percolated ionic conductor, the grey is the percolated electronic conductor and yellow is the un-percolated electronic conductor

Morphology

Table I presents the volume fractions of the phases and the percolating triple phase boundary length in these close packed structures. All data in the table is presented as the mean of 20 independent structures ± 1 standard deviation. The porosity and volume fractions are computed for the percolating clusters only, and hence they do not sum to 1. In all cases the pore phase is almost fully percolating and there is a slightly smaller volume of non-percolating ion conducting phase than electron conducting phase due to the addition of a thin solid electrolyte layer at the bottom of the electrode which ensures that all ion conducting clusters percolate at that boundary. The total volume fraction of the percolating phases is 0.96, 0.98, 1.0 for spheres agglomerates and cylinders, respectively. The resultant porosity decreases sharply as the aspect ratio of the base particles increases, and ranges from 0.37 for spheres to 0.16 for cylinders. The solid volume fractions are very close to equal in each case, and increase with increasing base particle aspect ratio from 0.29 to 0.42. On a normalized basis, the TPB more than doubles in the case of agglomerate geometries and increases by a factor of nearly 7 in the case of cylinders in comparison to the spherical cases.

TABLE I. Porosity, solid volume fractions and TPB density.

Geometry	Porosity	Ionic Vol. Frac.	Electronic Vol. Frac.	TPB [$\mu\text{m}/\mu\text{m}^3$]
Spheres	0.372 ± 0.0019	0.292 ± 0.0148	0.294 ± 0.0158	1.75 ± 0.083
Agglomerates	0.315 ± 0.0016	0.332 ± 0.0099	0.331 ± 0.0109	3.72 ± 0.077
Cylinders	0.163 ± 0.0021	0.418 ± 0.0105	0.414 ± 0.0113	12.2 ± 0.208

In Table II we provide the mean values of geometric tortuosity for the three phases and base particle shapes. The tortuosity of the pore phase is extremely low in the case of spheres and agglomerates and increases with increasing base particle aspect ratio, while the tortuosity of the two solid phases decreases. Here, the difference between sphere and

agglomerate structures is much smaller than the difference between agglomerate and cylinder structures. In the case of spheres and agglomerates the tortuosity of the solid phases dominates the tortuosity of the pore phase, in the case of cylinders the relationship is vice versa. Interpreting geometric tortuosity as a measure for the windedness of possible transport paths we can say that an increasing base particle aspect ratio has a positive effect on transport in the two solid phases but a negative effect on transport in the pore phase.

TABLE II. Mean geometric tortuosity.

Geometry	Pore Phase Tort.	Ionic Tort.	Electronic Tort.
Spheres	1.073 ± 0.00080	1.347 ± 0.039	1.339 ± 0.044
Agglomerates	1.089 ± 0.00088	1.269 ± 0.020	1.265 ± 0.026
Cylinders	1.252 ± 0.00341	1.158 ± 0.010	1.160 ± 0.012

TABLE III. Mean chord length.

Geometry	Pore Phase Chord L.	Ionic Chord L.	Electronic Chord L.
Spheres	0.426 ± 0.0035	0.658 ± 0.0037	0.659 ± 0.0037
Agglomerates	0.284 ± 0.0025	0.556 ± 0.0023	0.555 ± 0.0029
Cylinders	0.161 ± 0.0015	0.477 ± 0.0047	0.477 ± 0.0054

TABLE IV. Constrictivity.

Geometry	Pore Phase Constr.	Ionic Constr.	Electronic Constr.
Spheres	0.593 ± 0.0130	0.070 ± 0.0018	0.070 ± 0.0015
Agglomerates	0.584 ± 0.0101	0.093 ± 0.0034	0.094 ± 0.0017
Cylinders	0.312 ± 0.0134	0.712 ± 0.0188	0.728 ± 0.0276

Table III contains the mean chord length, which decreases in all three phases with increasing base particle aspect ratio. A decreasing mean chord length in the solid phases is natural because the particles are flattened in one direction; however, the drop in the mean chord length of the pore phase is even stronger, indicating that increasing the base particle aspect ratio leads even more to a refinement of the pore phase than to a refinement of the solid phases.

The values of constrictivity are given in Table IV. With increasing base particle aspect ratio, the constrictivity decreases in the pore phase and increases in the two solid phases. This means that bottle neck effects, which can be expected to hinder transport, become stronger in the pore phase and weaker in the solid phases, suggesting again that flattening the base particle shape improves transport in the solid phases and hinders transport in the pore phase.

Note that the geometric tortuosity, chord length and constrictivity of the ionically and electronically conducting phases should be almost the same since statistically, there is no difference between their geometries. Both are listed for the sake of completeness.

Transport and Electrochemical Performance

Table V presents the average of the directional transport coefficients normalized by the bulk value for the phase as well as the current produced in the electrode structure at a nominal over-potential of 0.1V. The pore phase effective diffusivity used in the transport simulations is further hindered by pore confinement effects represented by Kn and equation 2. Diffusive transport is significantly more hindered with increasing base particle aspect ratio (and reduced porosity) even more significantly than would be expected from porosity reduction without topological changes. Pore confinement effects also increase significantly with increasing base particle aspect ratio. The solid phase transport coefficient increases with increasing base particle aspect ratio, but not as significantly as the reduction in the diffusivity.

In the cases of spheres and agglomerates, the computed transport properties were found to be isotropic, while in the case of cylinders the transport coefficient in the direction of particle setting in the packing algorithm was found to be significantly lower.

TABLE V. Effective transport properties and current production.

Geometry	i [A/cm ²]				
	D/Do	Kn	σ_i/σ_{io}	σ_e/σ_{eo}	
Spheres	0.233 ± 0.0018	1.40 ± 0.012	0.026	0.028 ± 0.06	0.24 ± 0.016
Agglomerates	0.175 ± 0.0016	2.17 ± 0.016	0.041	0.043 ± 0.007	0.40 ± 0.023
Cylinders	0.023 ± 0.0011	3.87 ± 0.035	0.126	0.131 ± 0.013	0.80 ± 0.036

The current density produced in the electrode at a nominal over-potential of 0.1V indicates the combined effect of TPB density and transport through each of the three phases. Since the electronic conductivity is many orders of magnitude greater than ionic conductivity, the electron conducting phase contributes negligibly to the losses, and does not need to be solved (a constant value equal to the desired boundary condition can be used everywhere) while variations in hydrogen concentration through the pore phase contribute to a negligible loss in the case of spheres and approximately a 2% reduction in the total current in the case of cylinders. The total current produced increases by a factor of 1.7 and 3.3 in the case of agglomerates and cylinders respectively relative to spheres demonstrating that transport in the ionic conducting phase is critical to overall performance.

Figure 3 presents the local over-potential solved at the TPB, along with the percolating ion conducting phase. Further insight on the importance of ion transport can be gleaned from these result in noting that significant over-potentials exist at distances further from the electrolyte as the base particle aspect ratio and the ionic conductivity increases meaning that the volume of the electrode is better utilized in these cases.

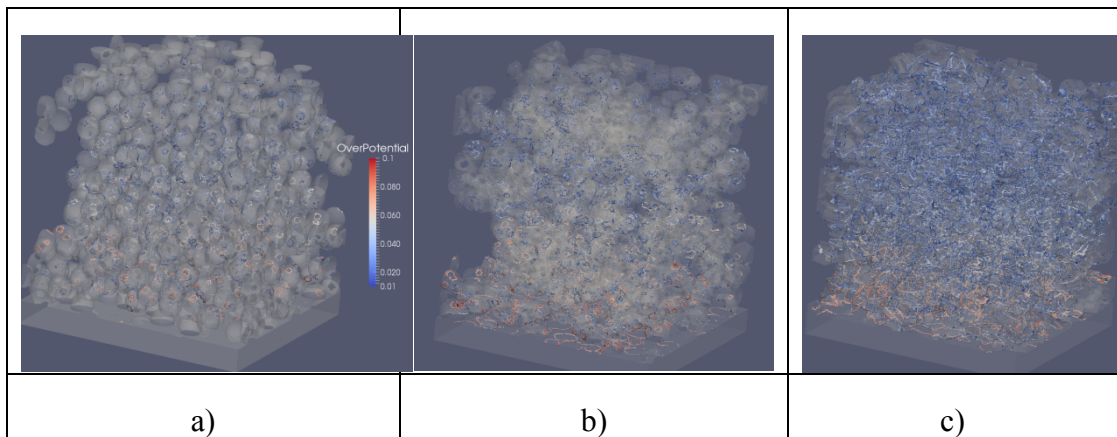


Figure 3. Local activation over-potential at the TPB in the cases of a) spheres, b) agglomerates and c) cylinders. The contour scale shown in a) applies to each sub-figure.

Conclusions

Three different classes of electrodes, with increasing base particle aspect ratio were generated and analysed in terms of geometrical properties, transport properties and electrochemical performance. Two analysis techniques were used, finite volume simulation and morphological characterization. It was found that with respect to close packed structures, the triple phase boundary length, the effective solid phase conductivity and the electrode performance increased with increasing base particle aspect ratio, while the pore phase effective diffusivity decreased with increasing base particle aspect ratio.

Morphological characterization is much more computationally efficient compared to the finite volume technique, and provides important information to elucidate the ultimate performance of solid oxide electrodes. In the present work, the constrictivity is the parameter which most closely correlates with the finite volume simulations of effective transport coefficients. Further work will be carried out to reliably predict transport performance from morphological characterization.

Acknowledgments

This work was supported by the German Academic Exchange Service (DAAD) providing travel funds for L. Handl and V. Schmidt.

References

1. B. Kenney, M. Valdmanis, C. Baker, J. G. Pharoah, and K. Karan, Computation of TPB length, surface area and pore size from numerical reconstruction of solid oxide fuel cell electrodes, *J. Power Sources*, **189**, 1051–1059 (2009)
2. H.-W. Choi, A. Berson, J. G. Pharoah, and S. B. Beale, Effective transport properties of the porous electrodes in solid oxide fuel cells, *Proc. Inst. Mech. Eng. Part A J. Power Energy*, **225**, 183–197 (2011)
3. M. Neumann, J. Staněk, O. Pecho, L. Holzer, V. Beneš, and V. Schmidt, Stochastic 3D modeling of three-phase microstructures with fully connected phases for simulation of Ni-YSZ anodes in solid oxide fuel cells (working paper)
4. G. Gaiselmann, M. Neumann, O. Pecho, T. Hocker, V. Schmidt and L. Holzer, Quantitative relationships between microstructure and effective transport properties based on virtual material testing, *AIChE J.*, **60**, 1983-1999 (2014)
5. J. Illian, A. Penttinen, H. Stoyan, and D. Stoyan, *Statistical Analysis and Modeling of Spatial Point Patterns*, J. Wiley & Sons, Chichester (2008)
6. S. N. Chiu, D. Stoyan, W. S. Kendall and J. Mecke, *Stochastic Geometry and its Applications*, J. Wiley & Sons, Chichester (2013)
7. A. Bertei, Chih-Che Chueh, J.G. Pharoah, C. Nicoletta, Modified collective rearrangement sphere-assembly algorithm for random packings of nonspherical particles: Towards engineering applications, *Powder Technology*, **253**, 311-324 (2014)
8. A. Berson, H.-W. Choi, and J. G. Pharoah, Determination of the effective gas diffusivity of a porous composite medium from the three-dimensional reconstruction of its microstructure *Phys. Rev. E*, **83**, 026310 (2011)
9. D. A. W. Gawel, J. G. Pharoah, S.B. Beale, Development of a SOFC Performance Model to Analyze the Powder to Power Performance of Electrode Microstructures, *ECS Trans.*, **this volume** (2015)
10. D. A. W. Gawel, *Queen's University Master's Thesis* (2013)
11. O. Stenzel, M. Salzer, V. Schmidt, P. W. Cleary, and G. W. Delaney, Quantitative structural analysis of simulated granular packings of non-spherical particles, *Granul. Matter*, **16**, 457-468 (2014)